

Efficient telecom to visible wavelength conversion in doubly resonant GaP microdisks

David P. Lake,¹ Matthew Mitchell,^{1,2} Harishankar Jayakumar,³ Laís Fujii dos Santos,⁴ Davor Curic,¹ and Paul E. Barclay^{1,2, a)}

¹⁾*Institute for Quantum Science and Technology, University of Calgary, Calgary, AB, T2N 1N3, Canada*

²⁾*National Institute for Nanotechnology, 11421 Saskatchewan Dr. NW, Edmonton, AB T6G 2M9, Canada*

³⁾*Department of Physics, City College of New York, New York, NY 10031, USA*

⁴⁾*Instituto de Física Gleb Wataghin, Universidade Estadual de Campinas, 13083-970 Campinas, São Paulo, Brazil*

Resonant second harmonic generation between 1550 nm and 775 nm with outside efficiency $> 4.4 \times 10^{-4} \text{ mW}^{-1}$ is demonstrated in a gallium phosphide microdisk cavity supporting high- Q modes at visible ($Q \sim 10^4$) and infrared ($Q \sim 10^5$) wavelengths. The double resonance condition was satisfied through intracavity photothermal temperature tuning using $\sim 360 \mu\text{W}$ of 1550 nm light input to a fiber taper and resonantly coupled to the microdisk. Above this pump power efficiency was observed to decrease. The observed behaviour is consistent with a simple model for thermal tuning of the double resonance condition.

Since the first observation of second harmonic generation (SHG) in 1961¹, it has become a ubiquitous demonstration of nonlinear optics. In recent years there has been mounting interest in SHG within micron-scale optical structures such as waveguides and cavities²⁻¹². These experiments seek to take advantage of devices whose combination of large optical quality factor, Q , and small mode volume, V , provide enhancements to electromagnetic per-photon field intensities at both fundamental and second harmonic wavelengths. Furthermore, the compact nature of these optical devices lends itself to convenient integration into complex on-chip photonic circuits. To date SHG has been demonstrated in a number of microresonator geometries including microdisks^{7,11-13}, microrings¹⁴, microspheres¹⁵, photonic crystal nanocavities^{5,6,8,9} and waveguides^{16,17}. An impressive $9 \times 10^{-2} \text{ mW}^{-1}$ conversion efficiency was achieved by Fürist et. al. in macroscopic (mm) sized whispering gallery mode resonators¹⁸. Conversion between 1985 nm and 993 nm light with outside and circulating efficiencies of $10^{-5} \mu\text{W}^{-1}$ and $10^{-3} \mu\text{W}^{-1}$, respectively, have been demonstrated in μm -scale gallium arsenide microdisks with low optical absorption at IR wavelengths¹². Microcavities have also been utilized in nonlinear optical processes including sum-frequency generation¹⁹, and third harmonic generation²⁰.

In this work we study microdisk cavities such as the device shown in Fig. 1(a), fabricated from gallium phosphide (GaP). The optical transparency window of GaP spans wavelengths from 550 nm to IR, making it a promising material for nonlinear wavelength conversion between C-band (1550 nm) and visible wavelengths⁸. Second harmonic conversion efficiency can be enhanced by fabricating microcavities supporting high- Q optical resonances at both pump (λ) and second harmonic wave-

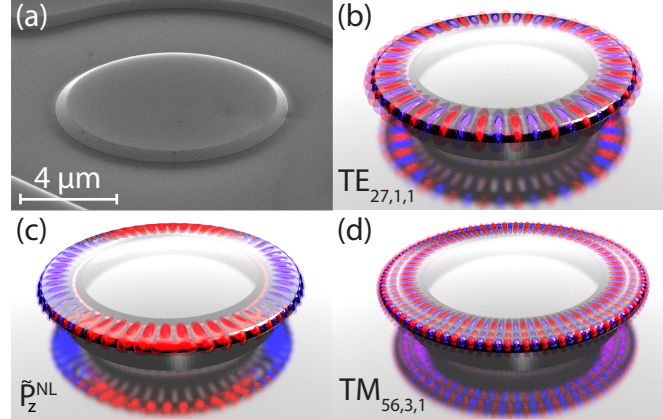


FIG. 1. (a) SEM of the device before undercut. (b) Visualisation of E_z , the \hat{z} -component fundamental mode. (c) z -component of the second order polarization driven by the electromagnetic field. (d) Visualisation of \tilde{H}_z , the \hat{z} -component fundamental mode. In (b-d) Blue represent positive regions, and red represents negative regions.

lengths ($\tilde{\lambda} = \lambda/2$). In principle this doubly-resonant condition can be satisfied through microcavity design by judicious choice of geometrical parameters. However, the high sensitivity of small- V devices to fabrication imperfections and variations in material optical properties, combined with the large free-spectral range of small- V structures, makes it challenging in practice to realize high- Q/V doubly-resonant microcavities. Existing approaches for addressing this problem include near-field perturbative tuning²¹, and bulk temperature tuning²². Here we demonstrate a method for tuning optical resonance wavelengths retroactively using dispersive intracavity photothermal effects, and utilize this tuning to enable highly-efficient conversion between $\lambda = 1545 \text{ nm}$ and $\tilde{\lambda} = 772 \text{ nm}$. By aligning high- Q resonances simulta-

^{a)}Electronic mail: pbarclay@ucalgary.ca

neously at λ_o and $\tilde{\lambda}_o = \lambda_o/2$, we demonstrate SHG with outside efficiency in excess of $4.4 \times 10^{-4} \text{ mW}^{-1}$.

Efficient SHG in microcavities requires, in addition to optical resonances at λ_o and $\tilde{\lambda}_o$, a phasematching mechanism. A common approach, known as quasi-phasematching, relies upon periodic domains with alternating nonlinear susceptibility²³. Interestingly, the zincblende structure of GaP possess $\bar{4}$ symmetry²³, which can be used to overcome dispersion intrinsic to the microdisk, and allow quasi-phasematching of microdisk whispering gallery modes without explicit creation of periodic domains^{10,12,24}. The microdisks studied here support high- Q radially polarized (TE) modes near λ_o , and high- Q TE as well as vertically polarized (TM) modes near $\tilde{\lambda}_o$. The second order nonlinear susceptibility of GaP couples TE modes at λ_o to TM modes at $\tilde{\lambda}_o$. These modes have azimuthal momentum whose field amplitude varies with $e^{im\theta}$, where m is the azimuthal number of the microdisk mode. Because of the vector nature of the electric field, the sign of the cartesian components, E_x and E_y , of the radially polarized TE mode changes with period $|\Delta\theta| = \pi$. The corresponding second order nonlinear polarization along z , $\tilde{P}_z^{\text{NL}} = 2\epsilon_0 d_{14} E_x E_y$ where d_{14} is the relevant nonlinear susceptibility tensor element of GaP, experiences a sign change with period $|\Delta\theta| = \pi/2$. This effect can be visualized from the isosurfaces of the microdisk electric field and \tilde{P}_z^{NL} , as shown in Fig. 1(b-d). Here Fig. 1(b) shows H_z of the fundamental mode, and Fig. 1(c) shows the corresponding \tilde{P}_z^{NL} generated by this field at an arbitrary point in time. In addition to the m label, the microdisk modes are indexed by p and q , which represent the number of radial and vertical antinodes, respectively. It can be seen that \tilde{P}_z^{NL} changes sign twice over a full rotation of the microdisk. This can be interpreted as momentum imparted by the periodic effective inversion of crystal orientation, creating azimuthal momentum components at $2m \pm 2$. As a result, the time-averaged coupling between \tilde{P}_z^{NL} and the dominant \hat{z} component of a TM polarized microdisk mode is maximized when $\tilde{m} = 2m \pm 2$, where \tilde{m} is the azimuthal index of the second harmonic mode¹⁰. This ± 2 offset can compensate for dispersion of the microdisk resonance frequency ω_o described by non-zero $\partial^2\omega_o/\partial m^2$.

The impact of the effects described above on the second harmonic power output by a microdisk are captured by¹⁰:

$$\frac{\tilde{P}_{f,b}}{P_f^2} = \delta\omega_{FSR}^2 |K|^2 \times \frac{\tilde{\lambda}_0/2\tilde{Q}_\kappa}{(\Delta\tilde{\lambda})^2 + (\tilde{\lambda}_0/2\tilde{Q}_t)^2} \left[\frac{1}{2} \frac{\lambda_0/2Q_\kappa}{(\Delta\lambda)^2 + (\lambda_0/2Q_t)^2} \right]^2. \quad (1)$$

where $\tilde{P}_{f,b}$ is the power output at second harmonic wavelength $\tilde{\lambda}$ into the forward and backward propagating modes, respectively, of a waveguide side-coupled to the microdisk, and carrying input power P_f . In the experiment described below, this waveguide is an optical fiber

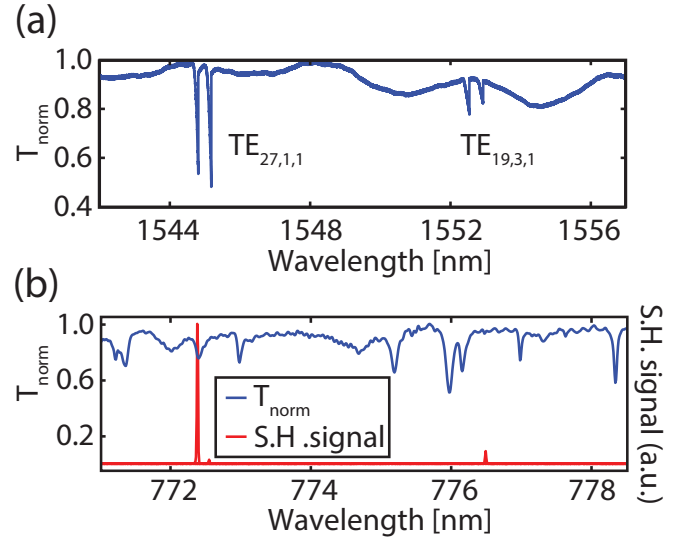


FIG. 2. (a) IR transmission of the modes of the 6.52 μm diameter disk. (b) Visible transmission of the same disk (blue) and corresponding second harmonic signal generated by input of IR light (red).

taper evanescently coupled to the microdisk. In deriving Eq. (1), we assumed that the λ_o resonance is a standing wave mode. As a result, SHG power is coupled into forward and backward propagating fiber modes. The second harmonic coefficient, K , given in the Supplementary Material, captures the material nonlinear susceptibility, the quasi-matching condition $2\tilde{m} = m \pm 2$, and the degree of spatial overlap between \tilde{P}_z^{NL} and the microdisk mode closest to $\tilde{\lambda}$. The resonant enhancement by the microdisk results in the product of Lorentzians whose maximum values depends on the loaded optical quality factors Q_t and \tilde{Q}_t , and the waveguide-cavity coupling quality factors Q_κ and \tilde{Q}_κ , of the pump and SHG field, respectively. The SHG efficiency is maximized when the doubly resonant condition is satisfied: $\Delta\lambda_o = \lambda - \lambda_o = 0$, and $\Delta\tilde{\lambda} = \tilde{\lambda} - \tilde{\lambda}_o = 0$, noting that $\tilde{\lambda} = \lambda/2$.

To achieve double resonance in micron sized devices, λ_o and $\tilde{\lambda}_o$ can be tuned differentially by varying P_f , which heats the microdisk due to intracavity optical absorption. Increasing the microdisk temperature T shifts λ_o and $\tilde{\lambda}_o$ due to thermal expansion and the thermo-optic effect. Differential tuning can arise from differences in modal confinement Γ , refractive index n_{GaP} , and thermo-optic coefficient dn/dT at λ_o and $\tilde{\lambda}_o$. The role of differential tuning on the SHG signal is determined by $\Delta\tilde{\lambda}_{\text{opt}} = (\tilde{\lambda}_0(P_f)/2 - \tilde{\lambda}_0(P_f))$, the detuning between the SHG and $\tilde{\lambda}_o$ when pumping ‘optimally’ on-resonance. The resulting SHG power is

$$\tilde{P}_{f,b} \propto \frac{\tilde{\lambda}_0/2\tilde{Q}_\kappa}{(\Delta\tilde{\lambda}_{\text{opt}})^2 + (\tilde{\lambda}_0/2\tilde{Q}_t)^2} P_f^2 Q_t^2 \left(\frac{Q_t}{Q_\kappa} \right)^2, \quad (2)$$

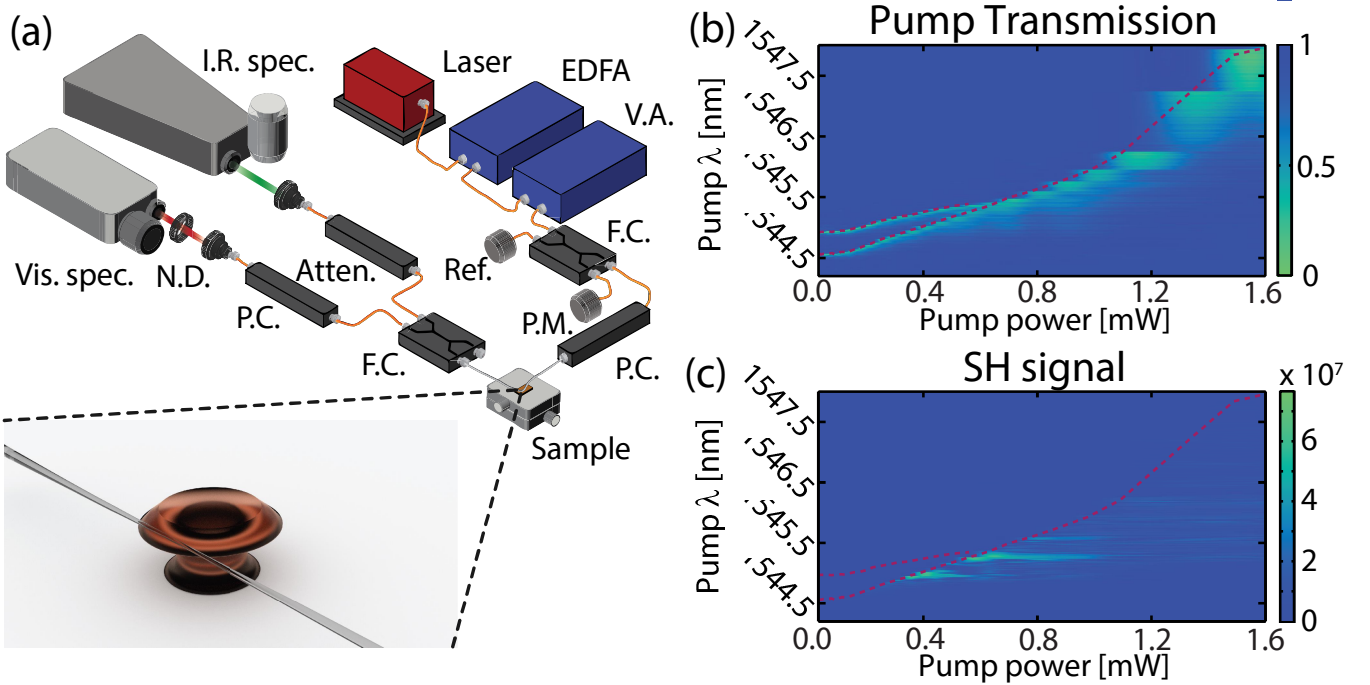


FIG. 3. (a) Setup for temperature tuning. Key: **Vis. spec.**: visible spectrometer, **I.R. spec.**: infrared spectrometer, **N.D.**: neutral density filter, **P.C.**: polarization control, **Atten.**: fixed attenuator, **F.C.**: fiber coupler, **P.M.**: power meter, **Ref.**: reflection intensity monitor, **V.A.**: variable attenuator, **EDFA**: erbium doped fiber amplifier. (b) Transmission through the optical fiber as a function of the P_f and λ . Thermal bistability is evident in the progression of the cavity resonance to longer wavelengths with increased pump power. (c) SHG signal corresponding to the pump laser shown in (b).

which for a given P_f , is maximum when $\Delta\tilde{\lambda}_{\text{opt}} = 0$. Assuming that the intracavity optical absorption is linear, $\Delta\tilde{\lambda}_{\text{opt}}$ is proportional to the circulating power $P_c = 4P_f Q_t^2/Q_\kappa$ in the standing wave microdisk mode. To reach $\Delta\tilde{\lambda}_{\text{opt}} = 0$, it is necessary that $d\lambda_0/dP_f \neq d\tilde{\lambda}_0/dP_f$. For the experiment described below, this differential tuning is dominantly provided by wavelength dependence of the normalized thermo-optic coefficient $(1/n_{\text{GaP}})dn_{\text{GaP}}/dT$. For GaP we calculate the normalized thermo-optic coefficients at λ_o and $\tilde{\lambda}_o$ to be $3.4 \times 10^{-5} [\text{K}^{-1}]$ and $2.9 \times 10^{-5} [\text{K}^{-1}]$ respectively²⁵, which leads to a differential tuning rate of 18%.

The microdisks used here for SHG were defined on a wafer consisting of a 250 nm layer of GaP on a 750 nm thick layer of aluminum gallium phosphide (AlGaP) following the process described by Mitchell et al.²⁶. Microdisks such as the devices shown in Fig. 1(a) prior to being undercut, with diameters from 6.5 μm to 7 μm were fabricated. To identify promising microdisks for efficient second harmonic generation, devices were characterized using fiber taper mode spectroscopy at IR wavelengths, while the spectrum of SHG produced by the

microdisk and collected by the fiber taper was simultaneously measured. Figure 2(a) shows the transmission through an optical fiber taper positioned in the near field of a 6.52 μm diameter microdisk, measured with $P_f \sim 0.5 \text{ mW}$ from a tunable IR wavelength laser (New Focus TLB-6700). Evanescent coupling from the fiber taper to high- Q microdisk doublet modes²⁷, resulting in sharp transmission dips, are clearly visible. Through comparison with finite difference time domain (MEEP) simulations of the microdisk mode spectrum measured from 1470 – 1570 nm, we identify each doublet as corresponding to TE-polarized modes with $\{m, p, q\} = \{27, 1, 1\}$ and $\{19, 3, 1\}$, respectively. We measured unloaded Q of 1.1×10^5 and 2.8×10^4 for the $p = 1$ and $p = 3$ doublets, respectively.

The integrated SHG spectrum measured from scanning the pump laser across each successive resonance is shown in Fig. 2(b). This was realized using a spectrometer configured as shown in Fig. 3(a). A 50:50 coupler, designed to split IR light and pass visible light, was connected between the fiber taper output and the spectrometer. The response of the spectrometer diffraction grating and CCD camera array prevented the IR pump from affecting the

visible second harmonic signals. Light at $\tilde{\lambda} \sim \lambda_o/2$, corresponding to the second harmonic wavelengths of the IR modes at wavelengths λ_o , was observed with varying intensity depending on the excited mode. This demonstrates the enhancement in second harmonic generation provided by large P_c from resonant excitation. Also evident is a significant variation of SHG depending not only on the mode type that is excited, but on the individual mode from a doublet pair that is excited. Since $|K|$ and P_c are equal for each mode of a doublet, this suggests that spectral alignment of $\tilde{\lambda}$ and $\tilde{\lambda}_o$ affects the SHG efficiency.

To study the alignment between the microdisk modes in the $\tilde{\lambda}$ range and SHG emission, we input broadband light from a supercontinuum laser (Fianium) to the fiber taper, and measured the resulting transmission using the visible wavelength spectrometer, shown in Fig. 2(b). Comparing the measured visible wavelength transmission with the second harmonic spectrum in Fig. 2(b), reveals that the strongest SHG occurs when $\tilde{\lambda} = \lambda_o/2$ is aligned with a resonance at $\tilde{\lambda}_o \sim 772.2$ nm with $\tilde{Q} \sim 9600$. In contrast, emission from the other mode in the doublet is off resonance.

To confirm that the high- \tilde{Q} optical mode is responsible for the strong SHG, we varied P_f while scanning λ of the IR pump across λ_o . This resulted in P_f and λ dependent heating of the microdisk, and provided a measurement of $\tilde{P}(\Delta\tilde{\lambda}_{\text{opt}})$. The IR laser was amplified using an erbium doped fiber amplifier (EDFA), whose output was controlled using a digital optical attenuator. The resulting variable power had a stable spectral profile, which was monitored using an IR spectrometer connected to fiber taper output via the 50:50 fiber coupler. Pump transmission versus P_f and λ is shown in Fig 3(b); the corresponding SHG is shown in Fig. 3(c). Each point in Figs. 3(b) and 3(c) is the integrated intensity of the narrowband signal detected by the IR and visible spectrometers, respectively, at a given $\{\lambda, P_f\}$. The redshift and distortion of the resonance in the pump transmission spectrum with increasing P_f in Fig. 3(b) is a result of thermal tuning from heating of the microdisk by linear optical absorption. Figure 3(c) shows that the SHG is most intense when exciting the shorter wavelength mode of the IR doublet, consistent with the observation in Fig. 2(b). The second harmonic generation is most intense for pump power $P_f \sim 0.35 - 0.70$ mW, where λ_o is shifted to $\sim 1544.8 - 1545.3$ nm. This suggests that the microdisk is thermally tuned such that $\tilde{\lambda}_o \sim \lambda_o/2$ when pumping on-resonance at this input power. Above 0.7 mW, the SHG decreases, suggesting that the microdisk resonances have been shifted past each other and that $|\Delta\tilde{\lambda}_{\text{opt}}|$ is increasing with increasing P_f .

In Fig. 4(a), we compare the maximum efficiency for each P_f with a model derived from Eq. (2). Here efficiency is defined as \tilde{P}_f/P_f , where powers are measured in the fiber taper immediately before (P_f) and after (\tilde{P}_f) the microdisk, taking into account asymmetric fiber ta-

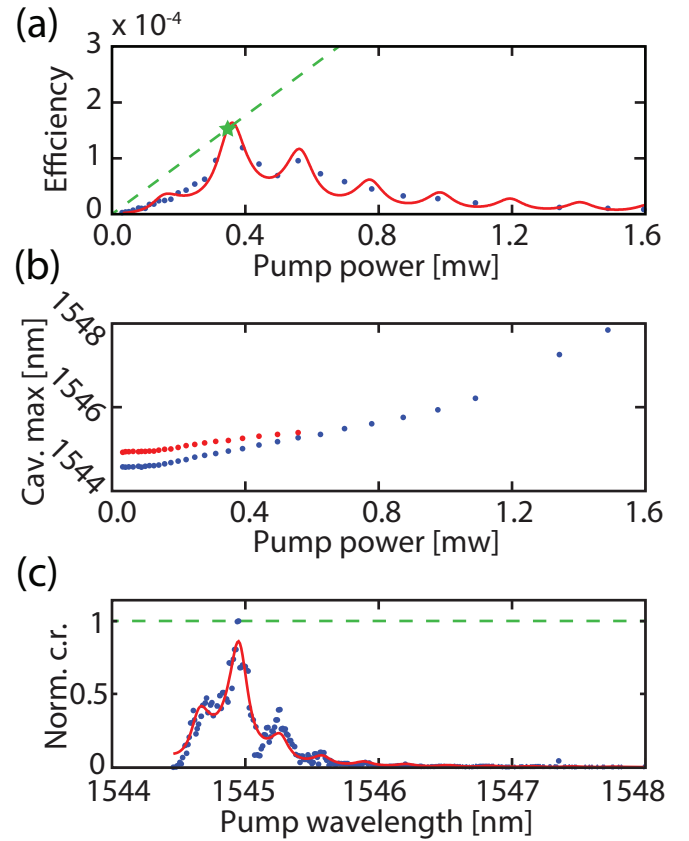


FIG. 4. (a) Maximum SHG efficiency versus P_f . The green star represents the data point with the highest efficiency, and the dashed green line represents the signal that would result if the outside efficiency remained constant. (b) Cavity resonance wavelength λ_o versus pump power P_f . For high P_f the doublet peaks can not be distinguished due to the thermal bistability of the microdisk. (c) Normalized SHG count rate ($\propto \tilde{P}_f/P_f^2$) plotted versus pump wavelength λ . The green dashed line represents the signal expected if the outside efficiency were a constant maximum value.

per insertion loss. The superlinear slope of the efficiency for $P_f < 0.35$ mW indicates a P_f dependent enhancement in the SHG efficiency in this region. A maximum normalized outside conversion efficiency was calculated to be 4.4×10^{-4} mW $^{-1}$ at an input power of 0.34 mW. Above this power, efficiency was observed to decrease. This non-monotonic behaviour is predicted by the model in Eq. (1), as shown in Fig. 4(a). This model treats the differential thermal tuning and initial mode detuning as fitting parameters which define $\Delta\tilde{\lambda}_{\text{opt}}$. Specifically, from the measured $\lambda_o(P_f)$, we assume $\tilde{\lambda}_o(P_f) = a_1\lambda_o(P_f) + a_0$ where a_1 and a_0 are fitting parameters. For reference, Fig. 4(b) shows the measured λ_o as function of P_f . In addition to including an overall scaling factor to represent various system efficiencies, a modification to account for etaloning caused by non-wedged neutral density filters used in the experiment was included in the fit. The mea-

sured SHG data is further analyzed in Fig. 4(c), which shows the maximum SHG signal at the optimal value of P_f for varying λ , normalized by P_f^2 . As in Fig. 4(a), the data was fit with the model from Eq. (2). From the differential tuning rate extracted from the fitting parameters, and the full-width at half-maximum of the data Fig. 4(c), we predict $\tilde{Q} \sim 1.0 \times 10^4$ of the visible wavelength resonance, in close agreement with the spectrometer measured value.

In conclusion, we have demonstrated resonant second harmonic generation from 1550 nm to 775 nm in a GaP microdisk with outside efficiency of 4.4×10^{-4} mW $^{-1}$, which is larger than previously reported outside efficiencies in similarly sized structures used for 2000 nm to 1000 nm wavelength conversion¹². We have shown that this efficiency is achieved via double resonance between high- Q modes of the GaP microdisk at both IR ($Q \sim 1.1 \times 10^5$) and visible ($\tilde{Q} \sim 1.0 \times 10^4$) wavelengths. Further improvements to the efficiency could be made by spectrally aligning higher- \tilde{Q} modes. Optimizing fiber taper coupling at visible wavelengths, and inserting an optical circulator to the excitation path to collect SHG coupled to the backwards propagating fiber mode would also improve efficiency. As GaP is a piezoelectric material, it may be possible to tune the modes through the application of an electric potential in the vicinity of the microdisks.²⁸ The geometry presented in this letter can also be adapted for use in other nonlinear optics scenarios such as four wave mixing and downconversion²⁹⁻³². With the present system we have already observed third harmonic generation, although efficient collection of the resultant 515 nm light via fiber taper requires additional optimization.

We would like to thank Aaron C. Hryciw, and J.P. Hadden for their assistance with this project. This work was supported by NRC, CFI, iCORE/AITF, NSERC, and CNPq.

- ¹P. A. Franken, A. E. Hill, C. W. Peters, and G. Weinreich, Phys. Rev. Lett. **7**, 118 (1961).
- ²S. Nakagawa, N. Yamada, N. Mikoshiba, and D. Mars, Applied Physics Letters **66**, 2159 (1995).
- ³J. Mondia, H. Van Driel, W. Jiang, A. Cowan, and J. F. Young, Optics letters **28**, 2500 (2003).
- ⁴V. S. Ilchenko, A. A. Savchenkov, A. B. Matsko, and L. Maleki, Phys. Rev. Lett. **92**, 043903 (2004).
- ⁵M. W. McCutcheon, J. F. Young, G. W. Rieger, D. Dalacu, S. Frédéric, P. J. Poole, and R. L. Williams, Phys. Rev. B **76**, 245104 (2007).
- ⁶S. Yamada, B.-S. Song, S. Jeon, J. Upham, Y. Tanaka, T. Asano, and S. Noda, Opt. Lett. **39**, 1768 (2014).
- ⁷S. Mariani, A. Andronico, O. Mauguin, A. Lemaître, I. Favero, S. Ducci, and G. Leo, Opt. Lett. **38**, 3965 (2013).
- ⁸S. Buckley, M. Radulaski, K. Biermann, and J. Vučković, Applied Physics Letters **103**, (2013).
- ⁹S. Dizaiain, R. Geiss, M. Zilk, F. Schremppel, E.-B. Kley, A. Tünnermann, and T. Pertsch, Applied Physics Letters **103**, 051117 (2013).
- ¹⁰P. S. Kuo and G. S. Solomon, Opt. Express **19**, 16898 (2011).
- ¹¹C. Wang, M. J. Burek, Z. Lin, H. A. Atikian, V. Venkataraman, I.-C. Huang, P. Stark, and M. Lončar, Opt. Express **22**, 30924 (2014).

- ¹²P. S. Kuo, J. Bravo-Abad, and G. S. Solomon, Nat Commun **5** (2014).
- ¹³S. Mariani, A. Andronico, A. Lemaître, I. Favero, S. Ducci, and G. Leo, Opt. Lett. **39**, 3062 (2014).
- ¹⁴W. H. P. Pernice, C. Xiong, C. Schuck, and H. X. Tang, Applied Physics Letters **100**, 223501 (2012).
- ¹⁵J. L. Dominguez-Juarez, G. Kozyreff, and J. Martorell, Nat Commun **2**, 254 (2011).
- ¹⁶K. Rivoire, S. Buckley, F. Hatami, and J. Vučković, Applied Physics Letters **98**, 263113 (2011).
- ¹⁷K. Lenglé, L. Bramerie, M. Gay, J.-C. Simon, S. Combré, G. Lehoucq, and A. De Rossi, Applied Physics Letters **102**, 151114 (2013).
- ¹⁸J. U. Fürst, D. V. Strekalov, D. Elser, M. Lassen, U. L. Andersen, C. Marquardt, and G. Leuchs, Phys. Rev. Lett. **104**, 153901 (2010).
- ¹⁹S. Buckley, M. Radulaski, J. L. Zhang, J. Petykiewicz, K. Biermann, and J. Vučković, Opt. Lett. **39**, 5673 (2014).
- ²⁰T. Carmon and K. J. Vahala, Nat Phys **3**, 430 (2007).
- ²¹G. Shambat, K. Rivoire, J. Lu, F. Hatami, and J. Vučković, Opt. Express **18**, 12176 (2010).
- ²²S. Mariani, A. Andronico, A. Lemaître, I. Favero, S. Ducci, and G. Leo, Opt. Lett. **39**, 3062 (2014).
- ²³R. W. Boyd, *Nonlinear optics* (Academic press, 2003).
- ²⁴Y. Dumeige and P. Feron, Physical Review A **74**, 063804 (2006).
- ²⁵D. Yas'kov and A. Pikhtin, Materials Research Bulletin **4**, 781 (1969).
- ²⁶M. Mitchell, A. C. Hryciw, and P. E. Barclay, Applied Physics Letters **104**, 141104 (2014).
- ²⁷M. Borselli, *High-Q microresonators as lasing elements for silicon photonics*, Ph.D. thesis, California Institute of Technology (2006).
- ²⁸C. W. Wong, P. T. Rakich, S. G. Johnson, M. Qi, H. I. Smith, E. P. Ippen, L. C. Kimerling, Y. Jeon, G. Barbastathis, and S.-G. Kim, Applied physics letters **84**, 1242 (2004).
- ²⁹Q. Li, M. I. Davanco, and K. Srinivasan, in *CLEO: 2015* (Optical Society of America, 2015) p. JTu5A.43.
- ³⁰W. C. Jiang, X. Lu, J. Zhang, O. Painter, and Q. Lin, Opt. Express **23**, 20884 (2015).
- ³¹Z. Yang and J. Sipe, Optics letters **32**, 3296 (2007).
- ³²L. Helt, Z. Yang, M. Liscidini, and J. Sipe, Optics letters **35**, 3006 (2010).

I. APPENDIX

Assuming that the resonance at the fundamental frequency ω_0 is a doublet, we can write the mode amplitude, A , as²⁷:

$$A = \frac{-\kappa/\sqrt{2}S_f}{i(\Delta\omega) - \gamma_t/2}, \quad (\text{S1})$$

where S_f is the amplitude of the forward propagating mode in the fiber taper, κ is the waveguide-cavity coupling, $\Delta\omega$ is the laser-cavity detuning, γ_t is the energy decay rate of the cavity into all channels. Here $|A|^2$ is normalized to energy, and $|S_f|^2$ is normalized to power. As this mode is a standing wave, it can be written as a superposition of clockwise and counterclockwise propagating components. It can be shown that each of these components will drive a source term for clockwise and counterclockwise modes at $\tilde{\omega}_0 = 2\omega_0$ according to the expression:

$$\tilde{\zeta} = \frac{A^2 \delta\omega_{FSR}}{4\pi} \int_0^{2\pi} \left[K_+ e^{i(\Delta m+2)\theta} + K_- e^{-i(\Delta m+2)\theta} \right] d\theta \quad (\text{S2})$$

where $\tilde{\zeta}$ is the source term, $\delta\omega_{FSR}$ is the free spectral range of the microdisk at ω_0 , and K_+ , K_- are the second harmonic coefficients, and Δm is the mismatch in the azimuthal numbers of the microdisk at ω_0 and $\tilde{\omega}_0$, defined as $\Delta m \equiv \tilde{m} - 2m$. The explicit form of the second harmonic coefficients, as derived in¹⁰, may be written as:

$$K_+ = -\frac{d_{14}}{2\epsilon_0 \tilde{\omega}_0 n^4} \int_0^\infty \int_{-h/2}^{h/2} \rho \tilde{\psi} \left(\frac{m\psi}{r} + \frac{\partial\psi}{\partial\rho} \right)^2 dz d\rho \quad (\text{S3})$$

$$K_- = \frac{d_{14}}{2\epsilon_0 \tilde{\omega}_0 n^4} \int_0^\infty \int_{-h/2}^{h/2} \rho \tilde{\psi} \left(\frac{m\psi}{r} - \frac{\partial\psi}{\partial\rho} \right)^2 dz d\rho, \quad (\text{S4})$$

where n is the refractive index of GaP at ω_0 , and ψ , $\tilde{\psi}$ give the radial and vertical dependence of the \hat{z} -component of the modes at ω_0 and $\tilde{\omega}_0$. Here we have assumed the normalization conditions $\int |\psi|^2 dA = \delta\omega_{fsr}/2\pi$ and $\int |\tilde{\psi}|^2 dA = \delta\tilde{\omega}_{fsr}/2\pi$ where the integrals are taken over the infinite half-plane.

We write the amplitude of the second harmonic modes propagating in the clockwise and counterclockwise directions as:

$$\tilde{A}^{cw} = \frac{\tilde{\zeta}}{i\Delta\tilde{\omega} - \tilde{\gamma}_t/2} \quad (\text{S5})$$

$$\tilde{A}^{ccw} = \frac{\tilde{\zeta}}{i\Delta\tilde{\omega} - \tilde{\gamma}_t/2}, \quad (\text{S6})$$

where $\tilde{\gamma}_t$ is the energy decay rate of the loaded cavity around $\tilde{\omega}_0$, $\Delta\tilde{\omega}$ is the detuning $\omega/2 - \tilde{\omega}_0$ with ω representing the laser frequency.

Combining equations (S1), (S2), and (S5), and writing the decay rates in terms of their respective quality factors we arrive at a final expression in terms of $\tilde{P}_{f,b}$, the power in the taper at $\tilde{\lambda}/2$ in either the forward or backward direction and P_f , the power in the taper at λ :

$$\frac{\tilde{P}_{f,b}}{P_f^2} = \frac{\tilde{\lambda}_0/2\tilde{Q}_\kappa}{(\Delta\tilde{\lambda})^2 + (\tilde{\lambda}_0/2\tilde{Q}_t)^2} \left[\frac{1}{2} \frac{\lambda_0/2Q_\kappa}{(\Delta\lambda)^2 + (\lambda_0/2Q_t)^2} \right]^2 \delta\omega_{FSR}^2 |K|^2. \quad (\text{S7})$$

with:

$$K = K_+ e^{i\pi(\Delta m+2)} \text{sinc}[\pi(\Delta m+2)] + K_- e^{i\pi(\Delta m-2)} \text{sinc}[\pi(\Delta m-2)]. \quad (\text{S8})$$